

University of Louisville

ThinkIR: The University of Louisville's Institutional Repository

Electronic Theses and Dissertations

4-2018

Materials design with polylactic acid-polyethylene glycol blends using 3D printing and for medical applications.

Jeremiah R. Bauer
University of Louisville

Follow this and additional works at: <https://ir.library.louisville.edu/etd>



Part of the [Biology and Biomimetic Materials Commons](#), [Biomaterials Commons](#), [Biomechanical Engineering Commons](#), [Ceramic Materials Commons](#), and the [Polymer and Organic Materials Commons](#)

Recommended Citation

Bauer, Jeremiah R., "Materials design with polylactic acid-polyethylene glycol blends using 3D printing and for medical applications." (2018). *Electronic Theses and Dissertations*. Paper 2886.
<https://doi.org/10.18297/etd/2886>

This Master's Thesis is brought to you for free and open access by ThinkIR: The University of Louisville's Institutional Repository. It has been accepted for inclusion in Electronic Theses and Dissertations by an authorized administrator of ThinkIR: The University of Louisville's Institutional Repository. This title appears here courtesy of the author, who has retained all other copyrights. For more information, please contact thinkir@louisville.edu.

MATERIALS DESIGN WITH POLYLACTIC ACID-POLYETHYLENE GLYCOL
BLENDS USING 3D PRINTING AND FOR MEDICAL APPLICATIONS

By

Jeremiah R. Bauer

B.S., University of Louisville, 2016

A Thesis

Submitted to the Faculty of the
Speed School of Engineering of the University of Louisville
in Partial Fulfillment of the Requirements
for the Degree of

Master of Engineering

in Mechanical engineering

Department of Mechanical Engineering

University of Louisville

Louisville, Kentucky

April 2018

Copyright 2016 by Jeremiah R. Bauer

All rights reserved

MATERIALS DESIGN WITH POLYLACTIC ACID-POLYETHYLENE GLYCOL
BLENDS USING 3D PRINTING AND FOR MEDICAL APPLICATIONS

By

Jeremiah R. Bauer

B.S., University of Louisville, 2016

A Thesis Approved on

April 24, 2018

by the following thesis committee:

Thesis Director
Kunal Kate

Sundar Atre

Jagannadh Satyavolu

ACKNOWLEDGMENTS

I would like to thank Dr. Kunal Kate for his leadership and insight in the writing of this thesis. I would also like to thank Dr. Sundar Atre, who first introduced me to the world of 3D-printing and materials science. I would like to thank the members of the MIG group, who have provided me with assistance and constructive criticism for both the research and in connected learning. I would like to thank my family for their encouragement and prayers during the writing process, especially my parents. Finally, I would like to give thanks to God for His guidance and blessings. Soli Deo Gloria!

ABSTRACT

MATERIALS DESIGN WITH POLYLACTIC ACID-POLYETHYLENE GLYCOL BLENDS USING 3D PRINTING AND FOR MEDICAL APPLICATIONS

Jeremiah R. Bauer

April 24, 2018

This thesis is an examination of two material systems derived from polylactic acid (PLA) and polyethylene glycol (PEG). PLA is a polymer commonly sourced from renewable sources such as starches and sugars. It is a relatively strong, biodegradable polymer, making it ideal for use in the body. Even though it has a relative high strength, PLA is also brittle leading to the use of plasticizers to increase flexibility. One such plasticizer is PEG, which is a material that can exist at room temperature as either a thin liquid, or a hard waxy solid depending on the molecular weight. The first chapter of this thesis introduces the goals of the second and third chapters by providing context to the two research projects that were done. The second chapter presents a study on the mechanical properties of 3D printed PLA-PEG blends, using two types of PLA and examining the effects of changing molecular weight of PEG and the concentration of PEG. The third chapter focuses on combining a modified PLA-PEG reaction blend with additional PLA and determining the dissolution profile, as this modified PLA-PEG blend shows some promise as a drug delivery material, due to how quickly it dissolves in water and phosphate buffered saline.

TABLE OF CONTENTS

ACKNOWLEDGMENTS	v
ABSTRACT.....	vi
TABLE OF CONTENTS.....	vii
LIST OF TABLES	ix
LIST OF FIGURES	x
CHAPTER I.....	1
Background and Goals.....	1
CHAPTER II.....	3
EFFECTS OF PEG MOLECULAR WEIGHT AND CONCENTRATION ON THE MECHANICAL PROPERTIES OF 3D PRINTED PLA-PEG BLENDS.....	3
2.1 Introduction.....	3
2.2 Materials and Methods.....	4
2.2.1 Extrusion.....	6
2.2.3 After-printed measurements.....	8
2.2.4 Tension testing.....	8
2.3 Results and discussion	9
2.3.1 Extruder torque	9
2.3.2 Printed tolerances.....	10
2.3.3 Tensile strength.....	11
2.3.4 Young’s modulus.....	13
2.3.5 Scaffold printing test.....	15
2.4 Conclusions.....	16
CHAPTER III	17
INFLUENCE OF PLA CONCENTRATIONS ON THE DISSOLUTION OF PLA-PEG BLENDS	17
3.1 Introduction.....	17
3.2.2 Reaction blending of PLA-PEG in an inert atmosphere for three hours.....	19
3.2.3 Blending of Material A with PLA.....	19
3.2.4 Molding of Material A and PLA blends	19
3.2.5 Density	19

3.2.6 Swelling	20
3.2.7 Dissolution Studies	20
3.2.8 UV Characterization	20
3.2.9 Fourier-transform infrared spectroscopy (FTIR)	21
3.3 Results and Discussion	21
3.3.1 Density	21
3.3.2 FTIR.....	22
3.3.3 Short term dissolution	24
3.3.4 Swelling of Blends.....	25
3.3.5 UV Spectroscopy	26
3.4 Conclusions.....	27
CHAPTER IV	28
OVERVIEW OF CONCLUSIONS	28
4.1 Conclusions from Chapter II.....	28
4.2 Conclusions from Chapter III	28
CHAPTER V	30
FUTURE WORK.....	30
5.1 Potential from Chapter II	30
5.2 Potential from Chapter III.....	30
APPENDIX.....	32
A. BIO-ABSORBABLE BONE REPAIR MATERIALS	32
A.1 Background	32
A.1.2 Preliminary research	33
A.1.2.1 Materials	33
A.1.2.2 Material property estimation	34
A.1.2.3 Blending and max solids loading	37
B. MINITAB PLA-PEG BLEND MECHANICAL PROPERTY MODEL.....	39
B.1 Minitab output.....	39
CURRICULUM VITAE.....	44

LIST OF TABLES

Table 1 Comparison table of common polymer properties.....	2
Table 2 Physical properties of PLA	5
Table 3 PEG molecular weights and physical states at room temperature	5
Table 4 Extruded blends of PLA and PEG	5
Table 5 Filament extrusion settings	6
Table 6 3D Printer settings	7
Table 7 Percent decrease in tensile strength from neat values.....	12
Table 8 Tensile strength factor correlation	12
Table 9 Percent decrease in Young's modulus from neat values	14
Table 10 Young's modulus factor correlation.....	14
Table 11 Planned UV characterization times.....	21
Table 12 PLA and copolymer blend densities	22
Table 13 UV absorptivity at 330nm.....	27
Table 14 Bone's mechanical properties.....	35
Table 15 Titanium's mechanical properties.....	35
Table 16 Estimated matching properties.....	36

LIST OF FIGURES

Figure 1. R. Scaffaro et al. PLA scaffolds.	3
Figure 2. 3D printer (left), dimensions (top right), and pattern example (bottom right).	7
Figure 3. Extruder torque.	9
Figure 4. Part tolerances.	10
Figure 5. Tensile strength by PEG concentration.	11
Figure 6. Young's modulus by PEG concentration (above), molecular weight (below).	13
Figure 7. Printed scaffold picture and SEM images.	15
Figure 8. PLA and PEG monomer diagrams.	18
Figure 9. FTIR results.	23
Figure 10. Short-term Dissolution results.	24
Figure 11. Swelling of Blends.	25
Figure 12. UV Spectroscopy results.	26
Figure 13. Hydroxyapatite particle size distribution.	33
Figure 14. Hydroxyapatite SEM image.	34
Figure 15. Average final mixing torques.	37
Figure 16. Mixing torque curve for 30% HA blend.	37

CHAPTER I

BACKGROUND AND GOALS

The materials of the ages have defined them to a great degree, such as the stone age, bronze age, and iron ages, but we are no longer bound to using a singular material to define the spirit of our age. There are millions of potential materials that humanity can choose from to solve any design problem. We are not only making use of discovered materials from nature but developing new material systems ourselves. From a strong and tough metal alloys to a soft and springy elastomer, there is potentially a perfect fit for every possible design. Since the beginning of man-made materials, we have added thousands to the list of available materials and slowly started to fully understand how best to use them. The biggest design challenge in deciding on a material is a lack of properties, mechanical or otherwise. Compounding this lack of material information is the possibility of mixing multiple materials into composites that should give the best of both materials, analogous to alloying metals. The methods of predicting the properties of compounds are estimates at best and guesswork at worst. In this work, we aim to fill a small void in the body of material properties within a specific group of materials.

The material system we consider is that of a biodegradable polymer polylactic acid (PLA), which is a plastic common to both the worlds of medicine and that of 3D printing, and polyethylene glycol (PEG) which is a material used as a plasticizer. PLA is strong compared to some polymers but lacks flexibility, a short list of some polymers is shown

below in Table 1 for comparison. To increase the flexibility of PLA, PEG is mixed with it PLA. PLA and PEG can also be processed under heat and an inert atmosphere to create what are called copolymers, where sections of one material's chain bond with a chain from the other.

Table 1 Comparison table of common polymer properties

Polymer	% Elongation	Tensile yield strength (MPa)	Tensile Modulus (GPa)	Biodegradable
PLA [1]	47.6	44.1	2.76	Yes
Polycaprolactone (PCL) [2]	674	27.3	0.378	Yes
Polyvinyl Chloride (PVC) [3]	224	50.4	2.7	No
Polypropylene (PP)	153	31.8	1.76	No

Both types of these materials will be examined. In Chapter II, a range of PLA and PEG blends will be considered. These blends use two types of PLA with different material properties and three molecular weights of PEG over three concentrations to determine the effects on material properties from each. In Chapter III, a modified PLA and PEG reaction blended material blended with additional PLA in two different concentrations. These two blends are compared with the original materials, the PLA, PEG, and the reaction blended PLA-PEG material to determine the dissolution properties

CHAPTER II

EFFECTS OF PEG MOLECULAR WEIGHT AND CONCENTRATION ON THE MECHANICAL PROPERTIES OF 3D PRINTED PLA-PEG BLENDS

2.1 Introduction

Medical materials have been under intense research as investment and interest are poured into solving common medical issues. M. Tobío et al. [4] studied the delivery of proteins using PLA-PEG nanoparticles through nasal membrane. As PLA-PEG blends are bio-absorbable, there is also some interest in using them to slowly deliver drugs over long periods of time. K. Kim et al. [5] studied the possibility of delivering antibiotics through a PLGA electrospun scaffold and used a PEG-b-PLA copolymer to better allow for long term release. T. Serra et al. [6] at the Institute for Bioengineering of Catalonia studied the 3D-Printing of very fine structured scaffolds using PLA and PEG with calcium phosphate to improve cell adhesion. R. Scaffaro et al. [7] at the University of Palermo, Italy studied the creation of scaffolds (pictured) containing micropores with PLA, PEG, and NaCl for

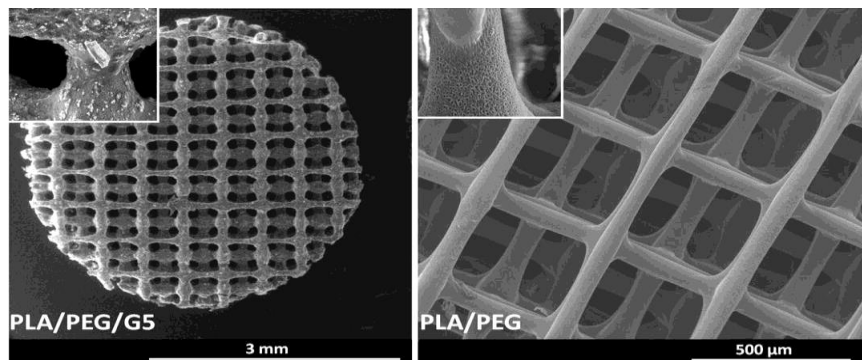


Figure 1. R. Scaffaro et al. PLA scaffolds.

tissue engineering through compression molding. Polymer-based composite systems can be made with extensive differences in properties and can be tuned with the addition of many more reinforcing materials, plasticizers, or medicines.

The specific material system considered in this work is a range of Polylactide (PLA) and Polyethylene glycol (PEG) blends, commonly used in 3D-printed cell tissue scaffolds. Combined with 3D-printing or other shaping methods, these materials may allow for patient-customized replacement tissue scaffold that automatically dose out medicine as they are harmlessly absorbed into the patient's body. Though this material system has been used in some research, material properties that consider the type of PLA and the type of PEG used, along with the effects of concentration, are not readily available.

2.2 Materials and Methods

Polylactide (PLA) is an opaque polymer commonly made from renewable feedstocks, such as corn starch. It is biodegradable, bio-absorbable, and FDA approved for use within the human body. Its material properties allow it to be used in some structural applications, as it has high strength, but it is limited primarily by a low flexibility. PLA is very capable of blending with many different additives to achieve improvements in the material properties. Depending on the molecular weight of the PLA, its melt flow index can be changed to better allow certain shaping methods to be used. Two blends of PLA were obtained from NatureWorks, LLC, one with a low melt flow index, PLA-3001D, and one with a higher MFI, PLA-3251D. Some of their properties are shown in Table 2.

Table 2 Physical properties of PLA

PLA blend	3001D	3251D
Melting temperature (°C)	200	188-210
Glass transition temperature (°C)	49.0	55-60
Crystalline transition temperature (°C)	155-170	155-170
Melt flow index @ 210°C (g/min)	1.1	8
Tensile yield strength (MPa)	62	62

Polyether glycol (PEG) is a material with various physical states depending on the molecular weight. Three molecular weights of PEG were obtained from Sigma-Aldrich, the physical state at room temperature shown in Table 3.

Table 3 PEG molecular weights and physical states at room temperature

PEG Molecular weight	600	1000	1500
Physical state (20°C)	Thick liquid	Waxy solid	

The PLA and PEG were blended in several ratios, using either one of the PLA types and one of the PEG molecular weights in batches of 5, 10, and 15% mass concentrations of PEG. The planned blends are shown in Table 4.

Table 4 Extruded blends of PLA and PEG

Batch	PLA Type	PEG MW	PEG m%	Batch	PLA Type	PEG MW	PEG m%
1	3001D	N/A	N/A	11	3251D	N/A	N/A
2	3001D	600	5%	12	3251D	600	5%
3	3001D	600	10%	13	3251D	600	10%
4	3001D	600	15%	14	3251D	600	15%
5	3001D	1000	5%	15	3251D	1000	5%
6	3001D	1000	10%	16	3251D	1000	10%
7	3001D	1000	15%	17	3251D	1000	15%
8	3001D	1500	5%	18	3251D	1500	5%
9	3001D	1500	10%	19	3251D	1500	10%
10	3001D	1500	15%	20	3251D	1500	15%

2.2.1 Extrusion

Each of the batches were hand-mixed in a container with the use of a hot-water bath to evenly coat the PEG across the PLA and extruded using a Brabender Intell-Torque single screw extruder. The extruder was controlled using Brabender WinExt software, which allowed modification of running settings in real-time. The extruder had four electrical resistance heated zones and was cooled with air to allow fine control of temperature. Additional device properties and running settings are shown in Table 5. The extruded filament was hand-spooled to produce a filament with an average diameter of 1.7 mm \pm 0.3 mm.

Table 5 Filament extrusion settings

Length/Diameter ratio	25:1
Diameter	0.75 in
Die shape	Circular
Die diameter	3 mm
Hopper heating zone temperature	160°C
Second heating zone temperature	160°C
Third heating zone temperature	155°C
Die heating zone temperature	150°C
Extrusion speed	24 rpm

2.2.2 3D Printing

A MakerGear M2 3D printer was used to print tensile coupons. The printer used featured a heated, glass bed and a 0.4mm extrusion nozzle. The standard filament size was 1.75 mm,

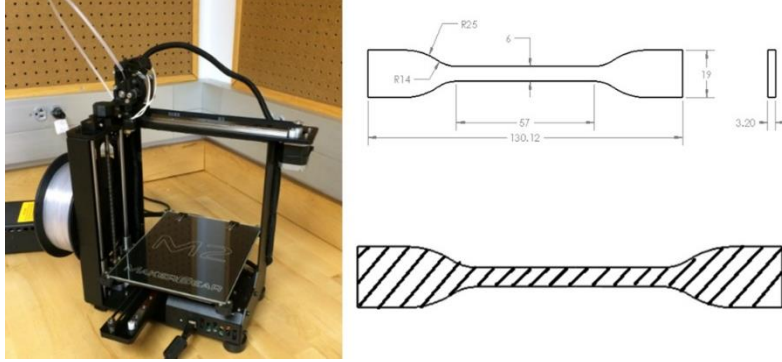


Figure 2. 3D printer (left), dimensions (top right), and pattern example (bottom right).

but readily accepted the prepared filament. The tension samples were designed to the dimensions of ASTM D638 type IV, as the smaller dimensions allowed for more samples to be made with lower printing times. 3600 mm of filament would have been needed to make a type I sample versus only 2000 mm of filament for the type IV, and the type I would have required 45 minutes to print versus the 23 minutes needed for a type IV. The tension bars were modified to have an additional 15 mm at the ends to better fit the available testing equipment. The printer was run using settings shown in Table 6. Standard print speeds, usually 30 mm/s, were reduced by 10% to better allow bed adhesion.

Table 6 3D Printer settings

Infill pattern	Rectilinear
Infill percentage	100%
Infill angle	45°
Hot end temperature	200-220°C
Bed temperature	50-65°C
Layer thickness	0.2 mm
Print speed	90% Program default

Each tension specimen used a 45° print angle, causing the rectilinear pattern to rotate completely every eight layers, an example of the pattern is shown in Figure 2. The rotation of the print pattern allows better use of directional strengths and better approximates a uniaxially strong part.

2.2.3 After-printed measurements

The parts were measured with digital calipers and compared with the design dimensions. The ends were measured for their width and thickness.

2.2.4 Tension testing

A MTI-2K tensile testing machine, was used to test all samples, with Epsilon extensometers of a gauge length of one inch. The tension specimens were labeled, and then were tested in random order, using a testing speed of 0.05 in/min, and removing the extensometer if the strain exceeded 3%. The testing speed was set to 0.2 in/min for samples with a large expected deformation.

2.3 Results and discussion

2.3.1 Extruder torque

The average extrusion torques are shown in Figure 3. Overall, a decrease was seen with increasing PEG, except in the 10% mass PLA 3251D and PEG 1000 or PEG 600. As

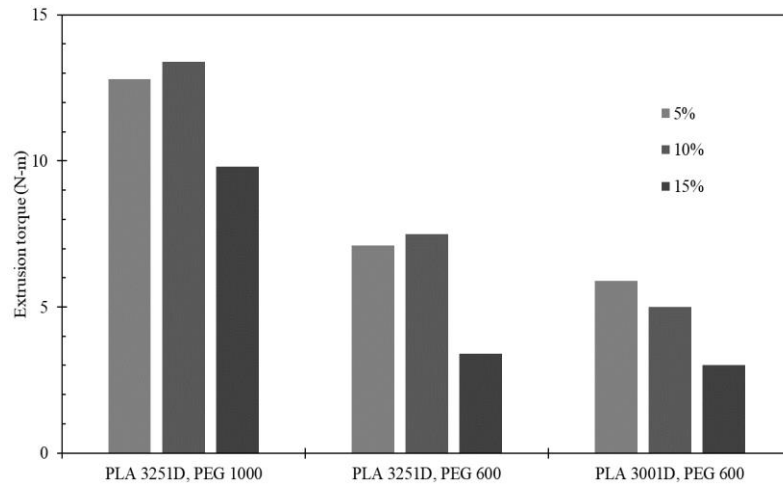


Figure 3. Extruder torque.

PEG molecular weight increased, the required torque increased. The lower molecular weight PLA required less torque to extrude than the higher molecular weight, at all mass percentages of the same molecular weight PEG.

2.3.2 Printed tolerances

The as-printed parts matched the target dimensions to within $\pm 0.25\text{mm}$. The most accurate parts within the weight percentages was the 10% for printed width and the 15%

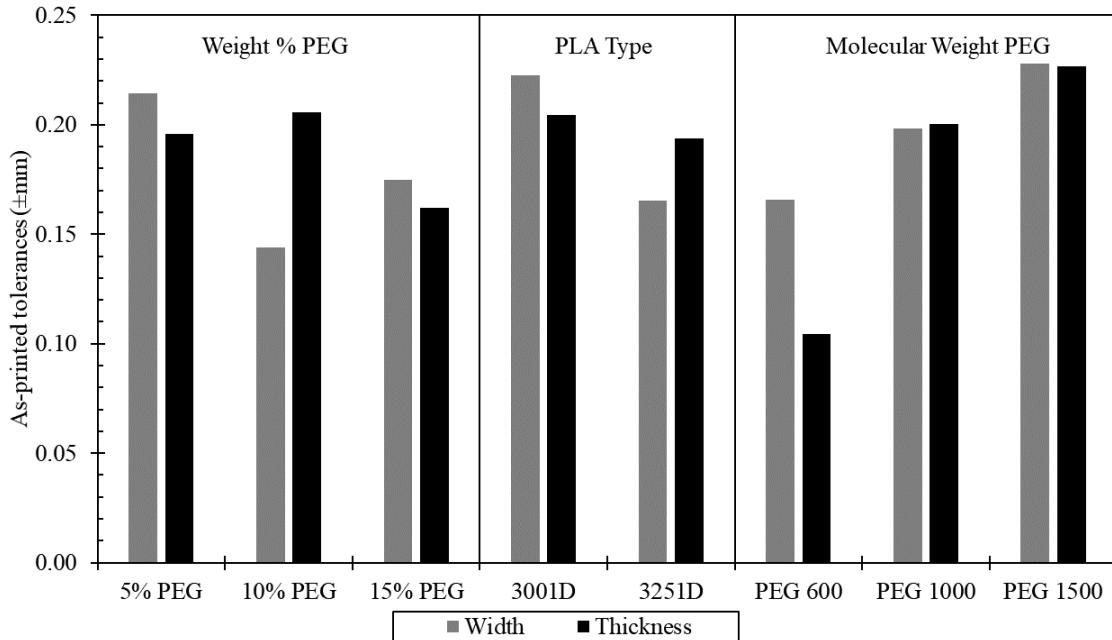


Figure 4. Part tolerances.

for printed thickness. Printing tolerances decreased with increasing PEG concentration. Between the two types of PLA, the 3251D was more accurate, most likely due to the increased viscosity inherent in the type of PLA. The lowest molecular weight PEG had the most accurate dimensions. The print tolerances increased with PEG molecular weight.

2.3.3 Tensile strength

The tensile strength of the blends all decreased from neat values with the addition of any molecular weight PEG, with higher mass fractions usually leading to reduced tensile

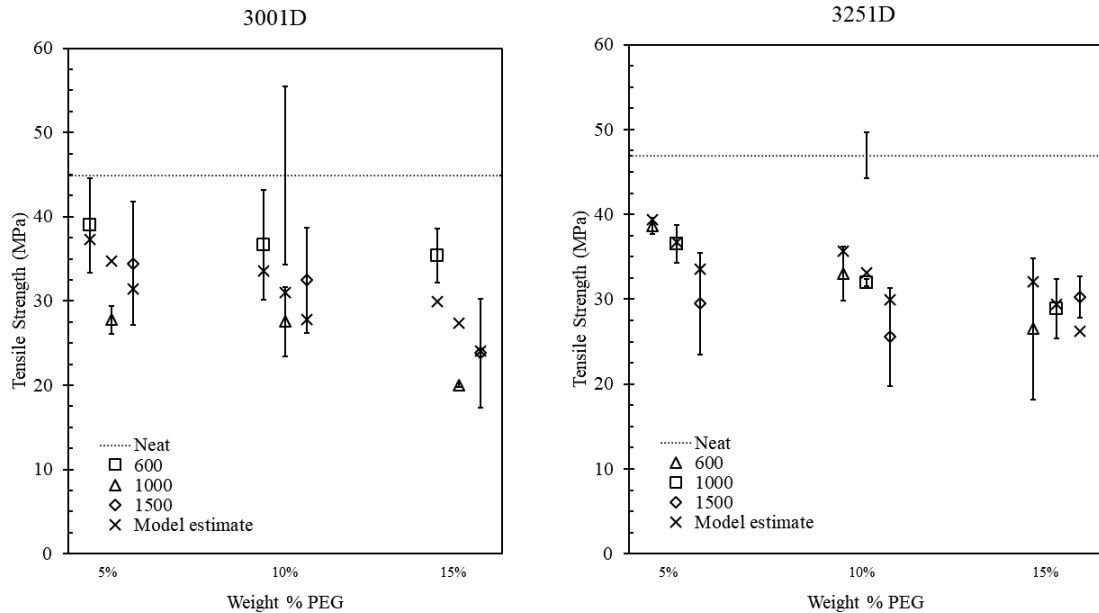


Figure 5. Tensile strength by PEG concentration.

strengths. Lower molecular weight PEG blends were more linear in their tensile strength reduction, whereas the higher molecular weight PEG blends did not follow a linear reduction, the 3251D and 1500 blend even showed a higher tensile strength at a 15% mass fraction. Tensile strength also decreased with the molecular weight of PEG, except for the 15% mass blend, where the PEG 1500 had a higher tensile strength than the PEG 1000. Overall, the 3251D was more affected than the 3001D by either an increase in weight percent or by an increase in molecular weight. An equation with the form

$$P = c - a * x_1 - b * x_2$$

was fit to the tensile strength data set using a regression model fit through Minitab, where P is the property being calculated, a , b , and c are constants, and the x terms are the

variables of interest, the PEG molecular weight and the weight percent. The constant c was set to the neat tensile strength of the blend of PLA, TS_{neat} , and the fitting gave the equation for tensile strength, TS ,

$$TS = TS_{neat} - 6.49 * 10^{-3} * MW_{PEG} - 73.5 * 10^{-2} * Wt\%_{PEG}$$

which is used to calculate the “Model estimate” points in Figure 5, where TS is MW_{PEG} is the molecular weight and $Wt\%_{PEG}$ is the weight percent of PEG. The r-squared value for the model was 70.9%, additional statistics are included in Appendix B.

Table 7 Percent decrease in tensile strength from neat values

	% Decrease from neat tensile strength					
	PEG Molecular weight			PEG Weight %		
PLA	600	1000	1500	5%	10%	15%
3001	19.3%	57.2%	39.9%	29.1%	33.4%	53.9%
3251	36.6%	36.9%	49.3%	30.0%	43.9%	48.8%

The drops in tensile strength for the 3251D were grouped more closely than the drops for the 3001D. The drops in tensile strength were not strictly increasing when considering the molecular weight of PEG but did increase with PEG weight percent. This is shown to a small degree by the correlation of the tensile strength to the PEG weight percent being slightly more negative than the molecular weight.

Table 8 Tensile strength factor correlation

Factor	Correlation
PLA Type	+0.04
PEG Molecular weight	-0.68
PEG Weight %	-0.73

The negative correlations for both PEG molecular weight and PEG weight percent to the tensile strength also demonstrate that increasing the molecular weight or the weight percent will lower the tensile strength. The type of PLA was not well correlated with the tensile strength but was barely positive in the favor of 3251D having an overall higher tensile strength.

2.3.4 Young's modulus

Young's modulus decreased with increasing mass percent PEG for nearly all blends, except the PLA 3251D and PEG 1500 blend where the 15% mass blend had a higher value than the 10% mass blend.

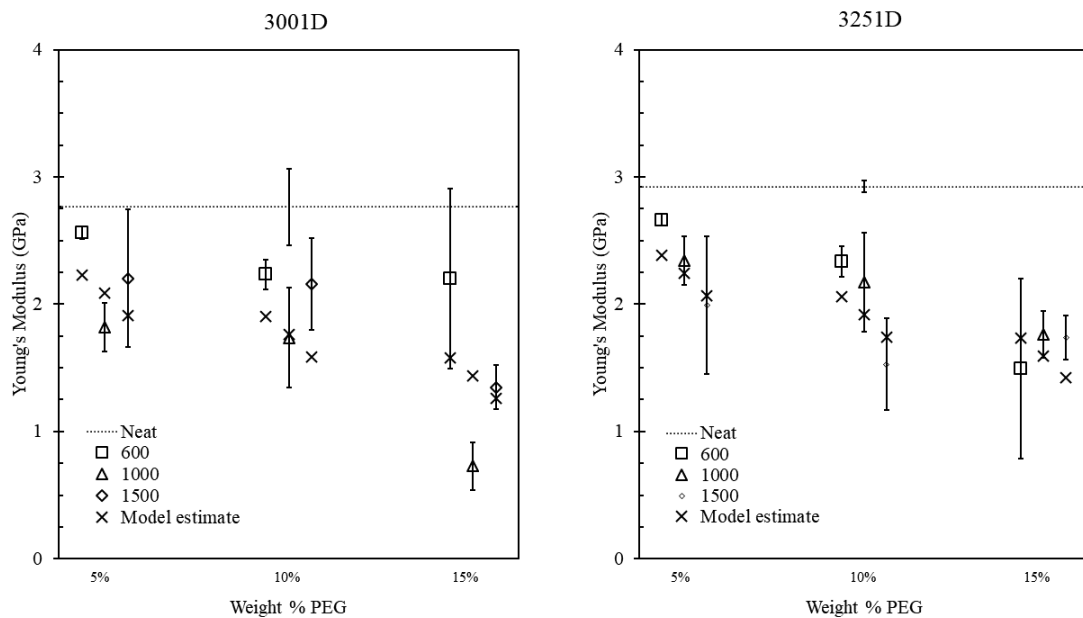


Figure 6. Young's modulus by PEG concentration (above), molecular weight (below).

With increasing PEG molecular weight there was a decrease in Young's modulus. The decreases in Young's modulus scaled with the increasing weight percent of PEG, but not with the molecular weight of PEG. The data was used to fit a predictive model using Minitab, much the same as the model for the tensile strength. The model was determined

by setting the constant to the neat value of the modulus of the PLA, E_{neat} , and was found to be

$$E = E_{neat} - 3.53 * 10^{-4} * MW_{PEG} - 6.5 * 10^{-2} * Wt\%_{PEG}$$

with a coefficient of regression, R^2 , of 65.4%.

Table 9 Percent decrease in Young's modulus from neat values

% Decrease from neat Young's modulus						
	PEG Molecular weight			PEG Weight %		
PLA	600	1000	1500	5%	10%	15%
3001	17.2%	67.8%	38.7%	23.8%	30.5%	69.5%
3251	32.1%	33.7%	50.5%	23.1%	38.2%	55.1%

The decreases in Young's modulus were not increasing in order within the 3001D and did not show much difference between the 600 and 1000 molecular weights within the 3251D. The increases in the drops from neat values did increase more regularly with weight percent.

Table 10 Young's modulus factor correlation

Factor	Correlation
PLA Type	+0.12
PEG Molecular weight	-0.57
PEG Weight %	-0.75

The correlation to the type of PLA was higher, but this mostly due to the much higher difference between the neat materials. Within Figure 6 above, the results were split evenly overall, neither PLA had a majority one way or the other within a blend. The effect of PEG molecular weight was less important than the weight percent, though the correlations of

both were not close enough to perfectly predict, the PEG weight percent did more strongly affect the Young's modulus.

2.3.5 Scaffold printing test

Several 9mm diameter scaffolds was printed with the 15% weight PEG, 1000 molecular weight, 3001D mixture. Below is a photograph of the scaffolds, in increasing

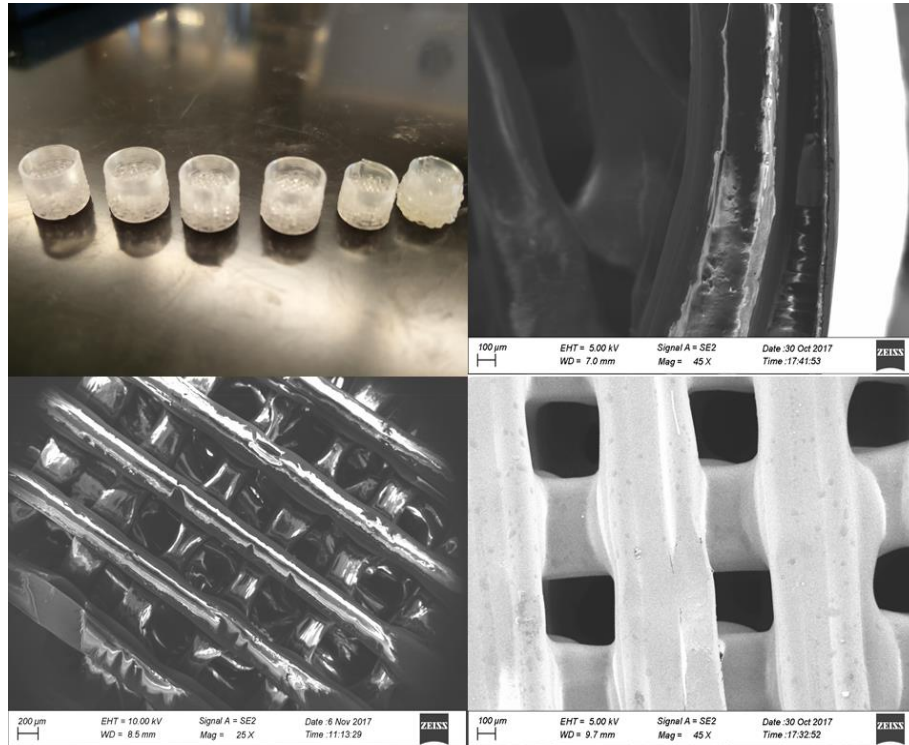


Figure 7. Printed scaffold picture and SEM images.

print accuracy from right to left, and three SEM image of the structure of the leftmost scaffold. A 0.1mm nozzle was used to print the scaffold as a 0.4mm nozzle was too large to capture the size of each individual line. The top right image shows the curvature of the scaffold and does not show any irregularities at the upper edge of the print. The bottom left image shows a regular and mostly evenly spaced grid. The final image on the bottom right shows slight pooling where the layers of the scaffold make contact, this demonstrating good interlayer bonding by showing clear contact between the layers.

2.4 Conclusions

Extrusion torque was lowered with increasing PEG weight percent and with PEG molecular weight. The printed tensile bars had good dimensional tolerances, falling within ± 0.25 mm in both width and thickness. The tensile strength decreased with increasing PEG mass percent and with PEG molecular weight. It did not always follow the trend for higher molecular weight and high mass percent blends. PEG molecular weight and weight percent negatively correlated with tensile strength and Young's modulus. PEG molecular weight was the weaker correlation in both circumstances, with the weight percent being the stronger, but not a perfect correlation.

CHAPTER III

INFLUENCE OF PLA CONCENTRATIONS ON THE DISSOLUTION OF PLA-PEG BLENDS

3.1 Introduction

Poly lactide (PLA) and polyether glycol (PEG) blends have been studied by several research groups across the globe, and have found to be usable in tissue engineering, wound healing, and in drug administration. Y.K. Luu et al. [8] at Stony Brook University studied the delivery of customized DNA in gene therapy through electrospinning PLA-PEG copolymer scaffolds, which approximated material properties for skin and cartilage. T. Kaito et al. [9] at Osaka University studied the introduction of bone morphogenic proteins to encourage bone growth in damaged sites with a PLA-PEG block co-polymer and hydroxyapatite ceramic additives. S. Venkatraman et al. [10] at Nanyang Technological University studied the delivery of chemotherapy drugs through PLA-PEG-PLA triblock copolymer. These examples are a short set of the potential of these polymer systems we see slowly unfolding as research continues in multiple areas.

As a part of this global research, this section will deal specifically with a PLA-PEG copolymer blended within a PLA structure. A 50% PLA, 50% PEG copolymer was synthesized and was shown to be water-soluble. The water-soluble property of the PLA-PEG copolymer is something that has not been explored within the context of a PLA blend. It is not understood how the dissolution is affected by the concentration of

the copolymer within the PLA, how the properties are affected, and how it can be tuned for a specific timed dissolution and chemical release. Current simple PLA and PEG mixtures do not have any significant surface or subsurface porosity, which is very important in the adhesion of cells to the polymer matrix. Using a mixture of PLA and the PLA/PEG copolymer system, we have created a material that can be shaped through similar processes as the base PLA (such as compression molding, injection molding, or 3D printing) and can then be placed in water, removing the copolymer and leaving behind a porous PLA lattice allowing for good cell adhesion while retaining the original strength of the PLA. Another possible use is in mixing drugs within both the copolymer and the PLA, allowing for two separate release schedules as the copolymer and the PLA follow a separate timetable for their dissolution.

3.2 Methods and Materials

3.2.1 Mixing and Molding

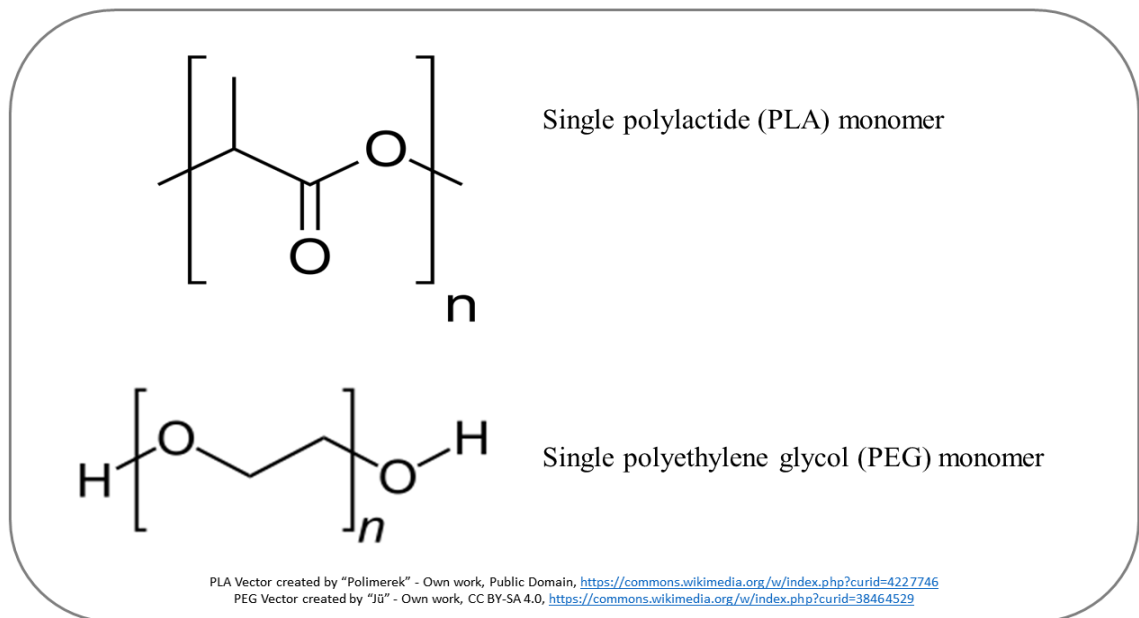


Figure 8. PLA and PEG monomer diagrams.

PLA (PLA-3001D) was acquired from NatureWorks, LLC. PEG of a molecular weight of 1000 was acquired from Sigma Aldrich. The chemical structures are shown above in Figure 8.

3.2.2 Reaction blending of PLA-PEG in an inert atmosphere for three hours.

A 1:1 blend of PLA and PEG was modified to create a copolymer system by melting and mixing the components and holding the mixture at 205°C under a nitrogen atmosphere for three hours, much like the process followed by J. Liu [11] to create a PLA-PET copolymer. The inert atmosphere was to prevent oxidative degradation of the PLA during the process. The copolymer, which we will refer to as Material A.

3.2.3 Blending of Material A with PLA

Material A was then mixed with additional PLA using a Brabender Intelli-Torque Plasticorder Prep Mixer to create two additional mixtures of 1:1 and 3:1 PLA to Material A, referred to as Blend 1 and Blend 2, respectively.

3.2.4 Molding of Material A and PLA blends

Using 15mm compression molding dies, each material system was cast into several 15mm diameter by 10mm high circular “pucks” to be used in testing. The molds were cleaned with soap and water, then rinsed with ethanol in between each molding. A light coat of mold release spray was used after cleaning to ensure even molding and easy removal.

3.2.5 Density

The material density was determined using a Micromeritics AccuPyc II 1340 gas pycnometer using helium gas. Four samples per material system were measured and three densities per sample were found using 10 trials each.

3.2.6 Swelling

The swelling ratio of the materials was found by measuring the initial mass before any fluid submersion. Individual beakers were filled with a Phosphate buffered solution and heated on a hot plate to body temperature (37°C). Four samples per material were submerged and the masses measured after 15, 30, and 60 minutes. The samples were dried on the outside with a paper towel before measuring the masses. The swelling was inferred from the increase in mass from the absorption of fluid.

3.2.7 Dissolution Studies

The short-term Dissolution profiles were found in both water and a phosphate-buffered saline solution at both room and body temperature up to a time of 240 minutes. Four samples per material blend were removed at 30-minute intervals, dried, and weighed. The mass lost was normalized to the average mass of the samples.

3.2.8 UV Characterization

UV spectroscopy was run for the materials by placing 4 samples per material blend and time measurement in separate beakers within a phosphate-buffered saline solution. The individual samples were kept in a Cole-Palmer StableTemp water bath isotherm chamber at 37°C. Fluid was removed from each sample at a specific time as per Table 11. Samples created from Material A were significantly dissolved at 4 hours and were not tested through the rest of the time samples. The fluid samples were run through a UV spectroscopy system and the absorptivity as a function of wavelength measured. The measured range was from 190 nm to 800 nm with a scan rate of 9600 nm/min, a data interval of 2 nm, and an averaging time of 0.0125 s. The machine was calibrated using DI water as a zero point and used a sample of the phosphate buffered solution as a baseline. Due to the number of

samples, plastic cuvettes were used that did introduce some noise underneath 300nm, and the data below this wavelength was discarded. Additional UV spectroscopy was done on PEG-1000 dissolved within PBS.

Table 11 Planned UV characterization times

Material blend		
Material A	Blend 1	Blend 2
2 hours	2 hours	2 hours
4 hours	4 hours	4 hours
N/A	6 hours	6 hours
N/A	12 hours	12 hours
N/A	1 day	1 day
N/A	3 days	3 days
N/A	7 days	7 days

3.2.9 Fourier-transform infrared spectroscopy (FTIR)

FTIR was done using a PerkinElmer Spectrum BX-FTIR for each of the material blends and the original materials. FTIR was done to give some evidence to show that Material A has some of the expected transesterification that would be seen in a copolymer.

3.3 Results and Discussion

3.3.1 Density

The expected densities of the mixtures, based on average densities of PLA 3001D and PEG-1000 were calculated using a weighted average of the total ratio of PLA to PEG to provide a limit for blends with an assumption of near-zero miscibility. As each blend was made using Material A, the measured densities were higher and reflected either a compaction expected by a copolymer, and/or more miscibility between the materials, as opposed to simple mixing with near-zero miscibility. The average densities are reported in Table 12 and are compared to the expected weighted average densities.

Table 12 PLA and copolymer blend densities

Sample	Measured density (g/cc)	Expected density (g/cc)	Difference
Material A	1.234	1.167	+ 5.58%
Blend 1	1.249	1.203	+ 3.75%
Blend 2	1.251	1.225	+ 2.10%

As more PLA was blended with Material A, the difference between the measured and expected decreased. The percent difference was roughly halved with the halving of Material A in Blend 1, and again in half with the halving in Blend 2, giving an indication that Material A was successfully blended.

3.3.2 FTIR

The Fourier-transform infrared spectroscopy results are presented in Figure 13 and shows the effects of the original ingredients in both the copolymer and the blends. Additionally, the peak shifts from the Carbonyl ester response range (1700-1750) toward the Hydroxyl group range (2600-3000) indicate that Material A is in fact a copolymer, though additional confirmation will be required to confirm this. Both blends inherited peaks from both Material A and from the neat PLA, showing that the blending was successful. Suppression of the peaks from Material A increased as the amount of PLA in the blend increased.

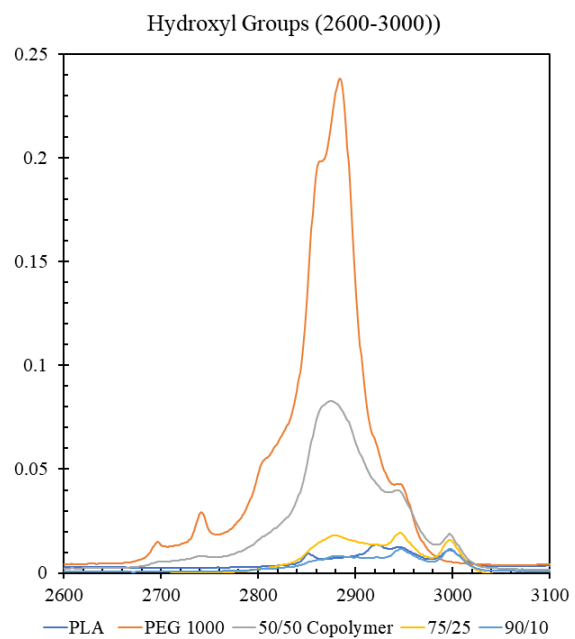
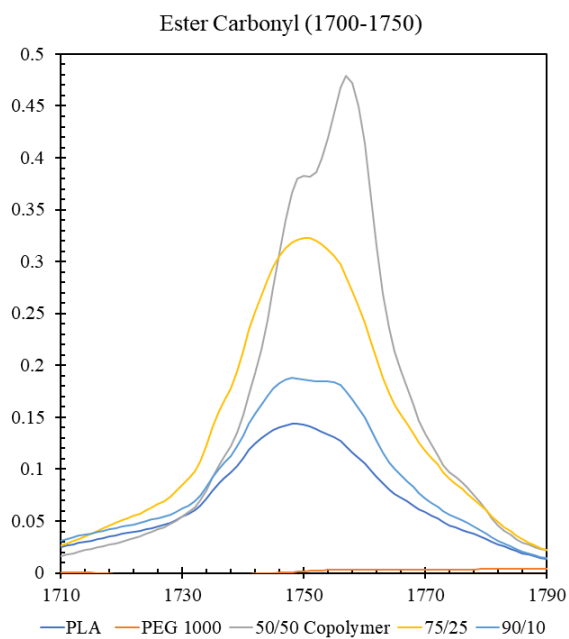
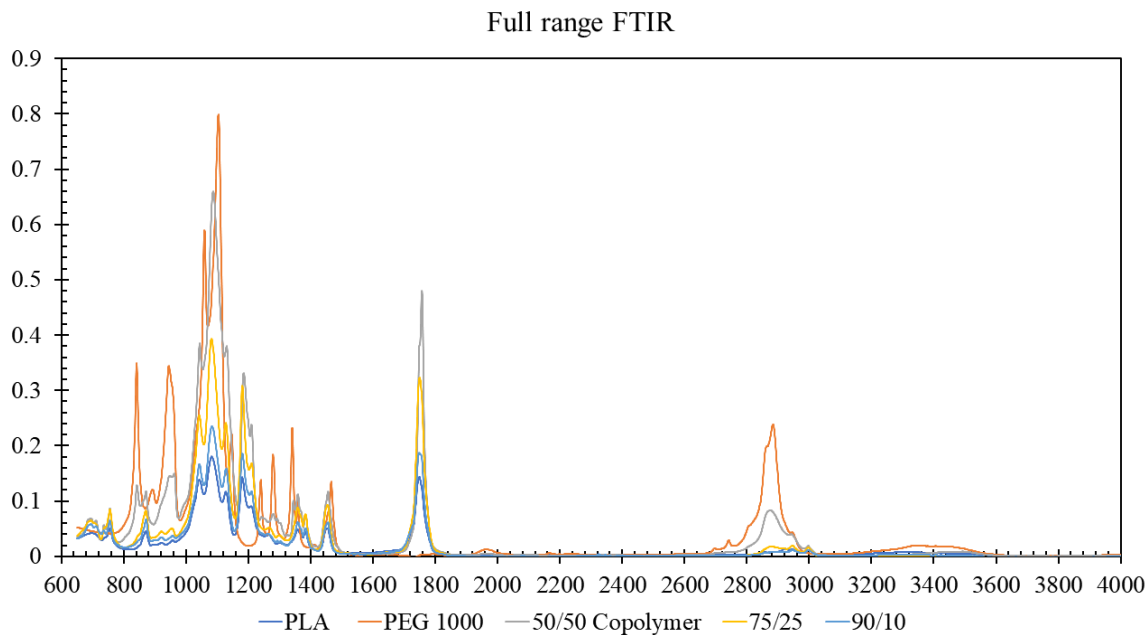


Figure 9. FTIR results.

3.3.3 Short term dissolution

The short-term dissolution for each sample is plotted in Figure 9. The Dissolution of Material A was significant in all mixtures and at all temperatures, showing the high water-

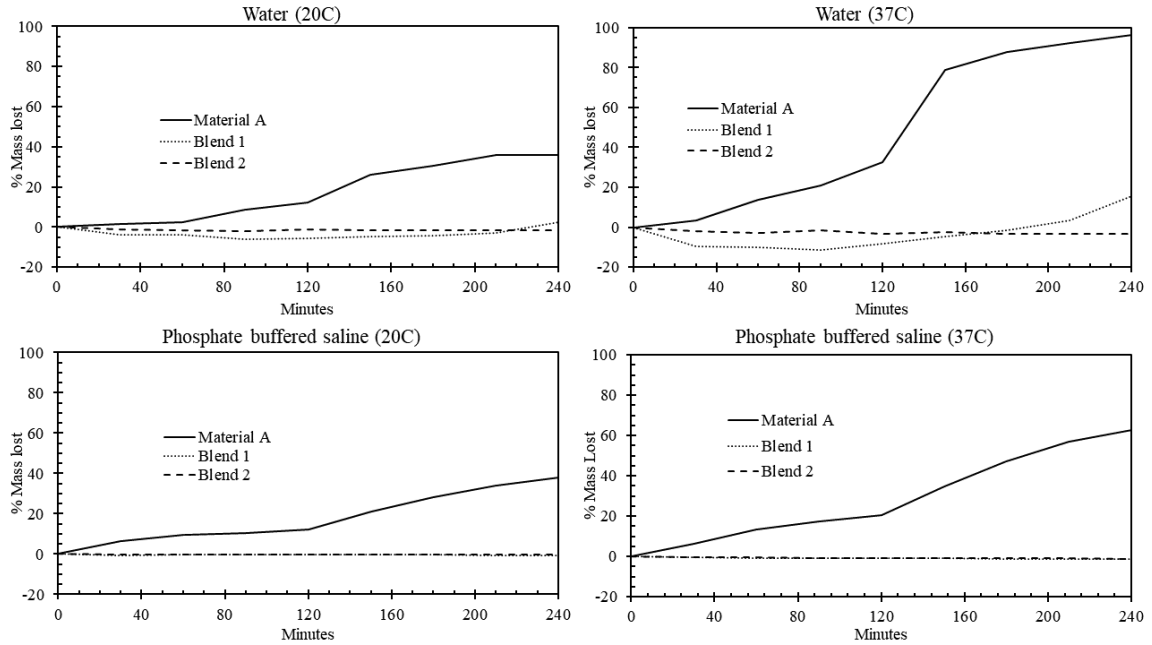


Figure 10. Short-term Dissolution results.

solubility of the material. The dissolution was more pronounced in deionized water, due to the lack of dissolved salts. The Material A sample was nearly completely dissolved within the 240 minutes in body temperature water versus in PBS which had lost 65% of its initial mass by the 240-minute mark. In the case of the PLA blends, the dissolution was much slower, and only showed mass loss within the DI water tests. Both blends showed swelling in the tests, discussed in 3.3.4. In the deionized water tests, Blend 2 did not lose any mass within the four hours. The PBS tests showed slight swell, but no dissolution of either blend.

3.3.4 Swelling of Blends

The swelling for Blends 1 and 2 are shown in Figure 10 in terms of the mass increase from the initial value within the degradation tests, from the degradation study in PBS at body temperature. Blend 1 absorbed more fluid than did Blend 2, but neither take in more than 1.5% of the original mass within the four hours.

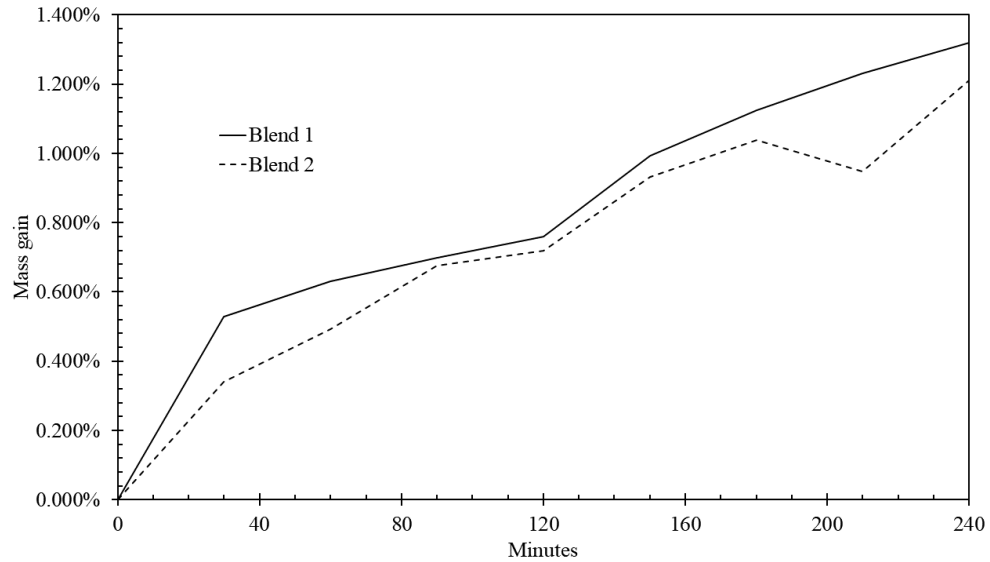


Figure 11. Swelling of Blends.

3.3.5 UV Spectroscopy

The absorptivity of PLA is higher than that of PEG, the absorptivity of PEG is shown in the uppermost image in Figure 11. The absorptivity of PLA, as shown by M. Nanda et al. [12], trends upward at the lower wavelengths, versus the PEG that trends downward from

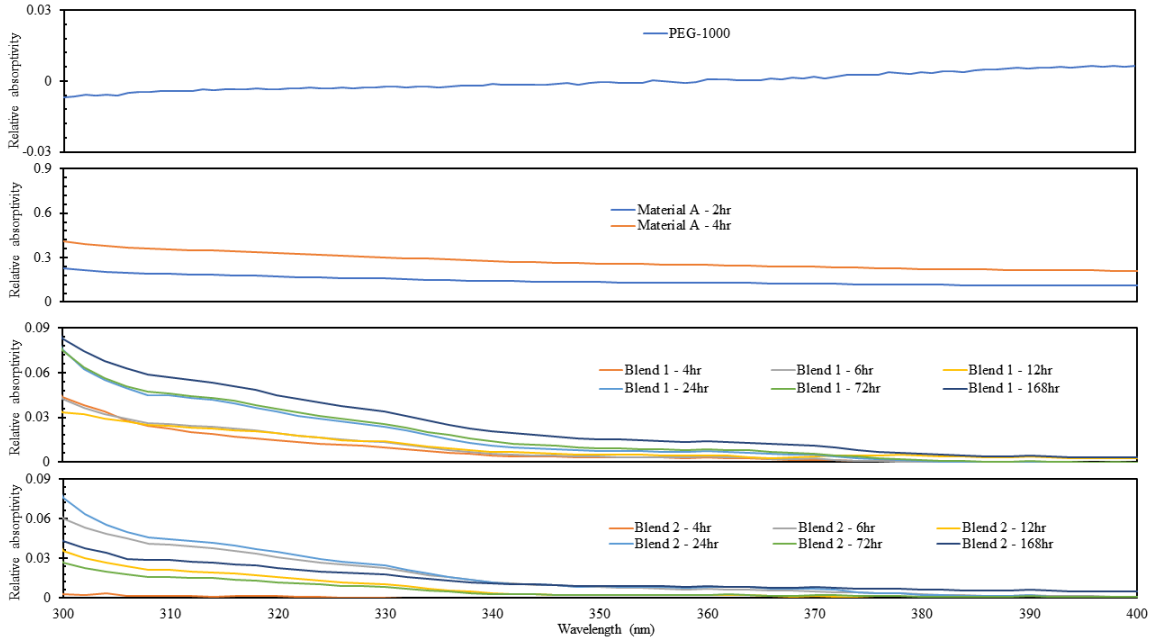


Figure 12. UV Spectroscopy results.

a peak at 400nm. From these, we can infer that any increase in the absorptivity is due to the presence of non-soluble PLA. The UV absorptivity of Material A increases over time as the material is dissolved into an opaque, cloudy fluid. The absorptivity of Blend 1 increases over time, especially obvious at 330nm. Blend 2 does not follow this pattern and the absorptivity does not increase over time. The relative absorptivity of the blends and the samples in chloroform at 330nm is shown in Table 13.

Table 13 UV absorptivity at 330nm

Relative absorptivity	2	4	6	12	24	72	168
Sample	Hours	Hours	Hours	Hours	Hours	Hours	Hours
Material A	0.1581	0.3032					
Blend 1	0.0509	0.0101	0.0132	0.0138	0.0236	0.0257	0.0339
Blend 2	0.0629	0.0002	0.0223	0.0103	0.0242	0.0083	0.0174

Material A has a doubling of the absorptivity between the two and four-hour tests. After an initial high absorptivity in Blend 1, there is a regular increase in absorptivity. In Blend 2, the same initial high absorptivity gives way to a disorganized set of absorptivities over time.

3.4 Conclusions

Material A and the Blends had a higher density than what would be expected from a near-zero miscibility blend of PLA and PEG, showing that it had blended the copolymer without drastically changing the original ratio. FTIR analysis showed some evidence of transesterification as would be expected in the formation of a copolymer, additionally, the FTIR showed both inherited peaks from Material A and suppressions from PLA that would be expected in the blended materials. Material A dissolved rapidly in body temperature deionized water and in PBS. The absorptivity of the Blend 1 followed a linear trend, while the Blend 2 followed no such trend.

CHAPTER IV

OVERVIEW OF CONCLUSIONS

4.1 Conclusions from Chapter II

In Chapter II, it was shown that the mechanical properties of the 3D printed PLA-PEG blends were in fact affected by both the molecular weight of the PEG and the weight percent of PEG in each blend. The type of PLA (3001D or 3251D) also affected the mechanical properties, most to a lesser degree than in the case of the molecular weight or the concentration.

The extrusion torque was lower using 3001D, as would be expected due to its lower melt flow index, but the torque was also decreased by higher molecular weights of PEG and their concentrations. The printed tolerances of all the parts were within 0.25mm of the original dimensions. Increasing the molecular weight of the PEG did somewhat lower printing tolerances but not consistently. The 3251D had tighter tolerances than the 3001D, due to a lower flowability. Increasing PEG molecular weight did have a deleterious effect on printing tolerances. Both tensile strength and Young's modulus were affected in the same way, with 3251D having an overall advantage and increasing molecular weight or concentration lowered the property value. The materials were successfully printed into a high-detail small structure with observed interlayer bonding at the edges of each layer.

4.2 Conclusions from Chapter III

In Chapter III, a potentially new material was created by thermal reaction blending and had some evidence from FTIR that there may potentially be transesterification between PLA and PEG. There was observed increased density in Material A, from either

compaction in copolymerization or a higher miscibility. This material was successfully blended with PLA to create two blends, 1:1 and 3:1, of Material A with the PLA. Material A was highly water soluble and dissolved rapidly in water and quickly in PBS, up to 96% in DI water and 63% in PBS within four hours. Higher temperature fluid increased the solubility of the material in both water and PBS, though more significantly in water due to the absence of salts. The two blends did not dissolve within the four hours of the test, and did absorb fluid, up to about 1.5% of their original mass, more significantly in Blend 1. The UV absorptivity of the surrounding fluids went up over time for both Material A and Blend 1. The fluid from Material A was opaque and a cloudy white. Blend 2 did not have a regular increase over time, most likely due to a lower concentration of Material A. The FTIR of the two blends showed the adoption of the peaks of their constituents and the suppression of some peaks with increasing PLA.

CHAPTER V

FUTURE WORK

5.1 Potential from Chapter II

There are several potential extensions of the work done in Chapter II. Work is still needed to improve the models for tensile strength and Young's modulus for both higher molecular weights and concentrations, possibly through the addition of thermal analysis. An examination of more types of PLA would also help fill in the gap of how the PLA was contributing to the changes in mechanical properties, outside of initial values.

Some work with the 3D printed scaffolds is currently being done at Alabama State to determine the effectiveness of the materials for culturing cells. An extension of this in the future would be to examine the effects of PEG molecular weight and concentration on the cultured cells, to be used in patient-specific skin grafting or tissue engineering.

5.2 Potential from Chapter III

The most important future work will start by confirming Material A as a copolymer through a combination of NMR and DSC/TGA. Some work the University of Louisville is being done in an attempt to 3D print Material A, using a heated syringe to extrude the material, but this is still in development to determine process parameters for an accurate print. The printed Material A may potentially be used for short term drug delivery. Additionally, the blended materials can be extruded into filaments for 3D printing, though the same process to determine the printing parameters would need to take place. As the blends did not fully dissolve within the four hours, extended time tests could be done to determine the full timetable for dissolution. Furthermore, as these materials have potential

in medical applications, it will be necessary to determine the effects of the dissolved material on cell life, and to test the dissolution in vivo for both the materials and the blends.

APPENDIX

A. BIO-ABSORBABLE BONE REPAIR MATERIALS

A.1 Background

Bio-absorbable products have been the subject of much research, as current medical procedures can be vastly improved through their integration. As a short list, bio-absorbable polymers have been investigated for long term drug delivery [13], facial fracture fixation plates [14], bone screws [15], and stents [16]. Titanium is currently used for many bone repairs because it is biologically inactive and extremely strong. These two factors represent significant drawbacks when seen from another angle. Bones increase and decrease in strength in response to external stresses imposed upon them. When a material with such high strength, like titanium, is used within bone, stresses are not experienced within the bone that otherwise would be felt as the high strength material absorbs a majority of the stress. This biological reaction is referred to as stress shielding and is the major drawback of using any high strength material compared to the natural strengths of bone [17]. Titanium is also bioinert, a great positive when trying to avoid infection or inflammation due to biological Dissolution but presents a drawback in that it will never naturally leave the body. Screws, plates, and pins used temporarily to repair damage need a secondary surgery to remove and thus require another surgery and introduce another chance that something goes wrong.

Bio-absorbable materials can bypass the second surgery, as they naturally dissolve and are absorbed into the body and can be tuned to match the material properties of bone, preventing stress shielding from occurring during the healing process. The materials chosen for this study are PLA, a bio-absorbable polymer currently used in many medical applications, and hydroxyapatite, a ceramic chemically similar to the naturally occurring apatite crystals in bone. The blending of these materials combines the high strength of the ceramic with the bio-absorbable property of the polymer matrix.

A.1.2 Preliminary research

A.1.2.1 Materials

PLA 3001D was acquired from NatureWorks, LLC, along with a hydroxyapatite powder from a Chinese supplier. The hydroxyapatite was examined with a Sympatec R-series laser diffraction system to determine the particle size, the results of this are shown

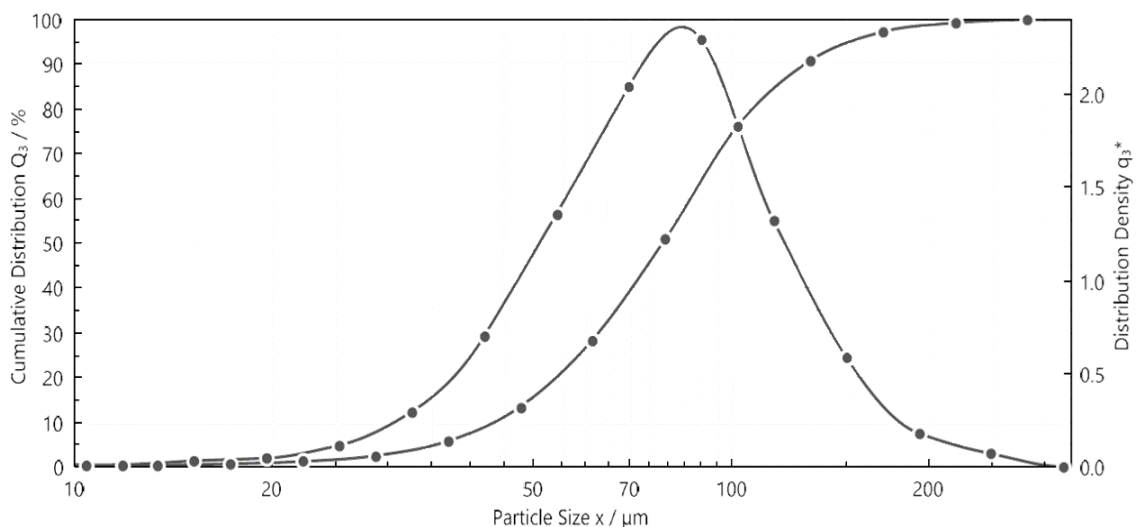


Figure 13. Hydroxyapatite particle size distribution.

below in Figure 15 The x_{50} from the LDS was $78\mu\text{m}$, showing that this was a small, but

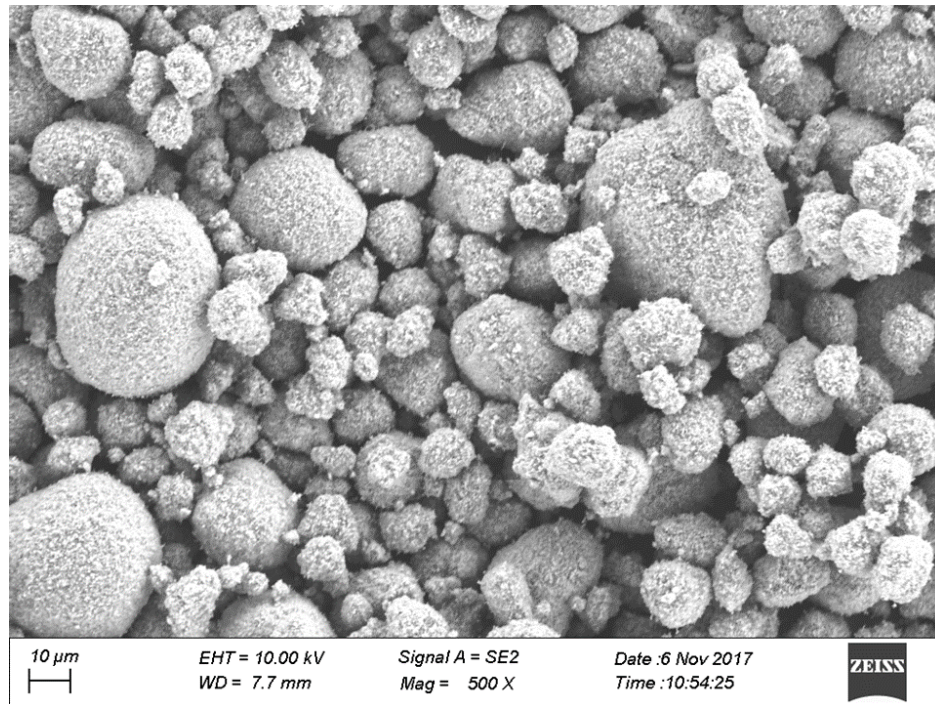


Figure 14. Hydroxyapatite SEM image.

comparatively large powdered hydroxyapatite. SEM imaging was done on a sample of the powder to confirm the general shape and check the particle size results of the LDS and is shown above in Figure 14. The SEM image shows that there are also a significant number of particles underneath the visible range of $10\mu\text{m}$ for the LDS system used.

These nanoparticles are closer to the size used in other research and appear to be a significant percentage of the particles imaged.

A.1.2.2 Material property estimation

The material property goals for the composite material were found through a review of several studies that had previously measured the significant properties of bone, namely the elastic modulus, compressive modulus, tensile strength, compressive strength, and density. The material property ranges are presented in Table 14 below.

Table 14 Bone's mechanical properties

Property [18], [19], [20]	Measured range
Ultimate tensile strength	125-175 MPa
Ultimate compressive strength	130-220 MPa
Tensile modulus	15-20 GPa
Density (dry)	1.32-2.10 g/cc
Density (wet)	1.61-1.99 g/cc

The material properties of bone are vastly below those of Titanium, some of which are presented in Table 15 below. The strength of titanium vastly outclasses bone in every measure, it is much stronger, is less flexible, and is more than twice as heavy.

Table 15 Titanium's mechanical properties

Property (Ti-6Al-4V) [21]	Value	Percent difference
Ultimate tensile strength	950 MPa	+ 137.8%
Tensile modulus	113.8 GPa	+ 140.2%
Density	4.43 g/cc	+71.4%

A material that better approximates the properties of bone will avoid the problem of stress shielding without sacrificing the strength to support damaged bone while it is healing.

The properties of the material blends of the polymer and ceramic composite were first estimated through the rule of mixtures, which is a bounded prediction of the possible range of material properties. The upper bound is found using

$$P_C = X_f P_f + (1 - X_f) P_m$$

and the lower bound is found using

$$P_C = \left(\frac{X_f}{P_f} + \frac{1 - X_f}{P_m} \right)^{-1}$$

where the X_f term refers to the volume fraction of the composite and the P_f and P_m terms refer to the properties of the filler and the polymer matrix, respectively. Using published values for all mechanical properties, the estimated properties of the blended composite were calculated and are shown in Table 16 where at what volume fraction of hydroxyapatite the material blend would theoretically match the material property of bone.

Table 16 Estimated matching properties

Property	Matched volume fraction
Ultimate tensile strength	40-80%
Ultimate compressive strength	10-35%
Tensile modulus	15-85%
Density	20-40%

While there is not a perfect match, a range of 20-40% captured at least three of four. At the upper ranges of hydroxyapatite volume fraction, the predicted strength was more than what was required, and at lower volume fractions, the composite was not predicted to have the strength to be close to the properties of bone.

A.1.2.3 Blending and max solids loading

The materials to blend were as follows, 20%, 30%, and 40% hydroxyapatite by volume, PLA, and 0.5% by mass stearic acid as a surfactant to ensure equal and thorough blending. The mixtures were blended in a Brabender IntelliTorque Prep-Mixer with a twin-screw Prep-Mixer attachment. The mixing torque was captured over time for each mixture. A sample pattern is shown in Figure 16 below where the initial spike in torque is the time

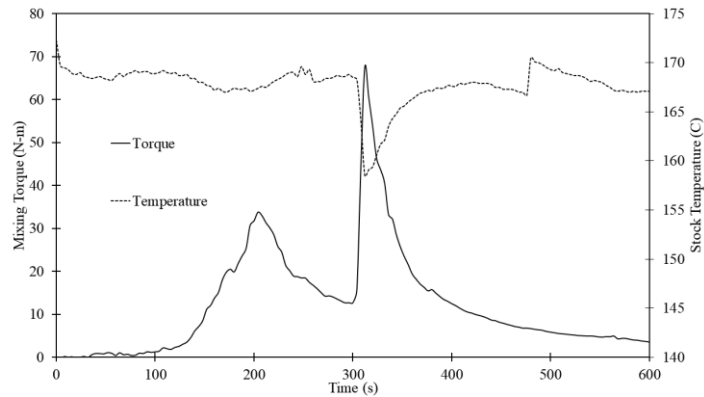


Figure 16. Mixing torque curve for 30% HA blend.

at which the PLA first begins to melt, and the second spike is the introduction of the

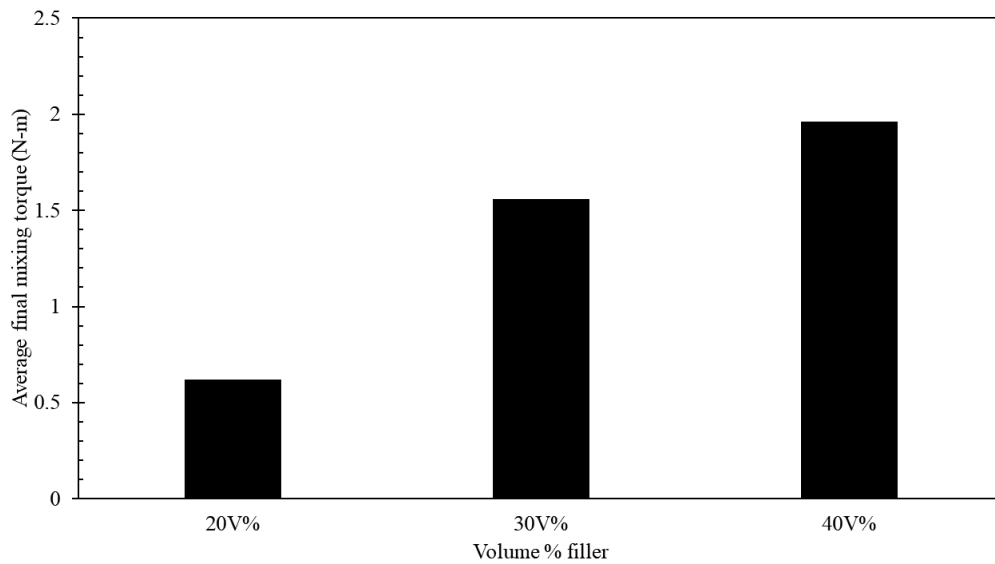


Figure 15. Average final mixing torques.

hydroxyapatite powder to a molten PLA. The torque eventually settles to a stable number given enough time, average torques measured for each mixture are shown in Figure 17. As can be seen, there is a decreasing rise in average final mixing torque with the addition of filler, indicating that the maximum solids loading is being approached where the introduced powder will be unable to be absorbed into the matrix due to oversaturation. A simple 2nd degree function fit to the average mixing torque predicts that the maximum solids loading may occur at around 62.5% volume filler load, but this value may under-predict the actual maximum.

B. MINITAB PLA-PEG BLEND MECHANICAL PROPERTY MODEL

B.1 Minitab output

Regression Analysis: Avg. TS (Mpa) versus PEG, WT (%), PLA

Method

Categorical predictor coding (1, 0)

Analysis of Variance

Source	DF	Adj SS	Adj MS	F-Value	P-Value
Regression	3	621.517	207.172	13.00	0.000
PEG	1	153.174	153.174	9.61	0.007
WT (%)	1	216.257	216.257	13.57	0.002
PLA	1	1.708	1.708	0.11	0.748
Error	16	255.044	15.940		
Total	19	876.561			

Model Summary

S	R-sq	R-sq(adj)	R-sq(pred)
3.99252	70.90%	65.45%	54.68%

Coefficients

Term	Coef	SE Coef	T-Value	P-Value	VIF
Constant	44.83	2.40	18.67	0.000	
PEG	-0.00649	0.00209	-3.10	0.007	1.20
WT (%)	-0.735	0.199	-3.68	0.002	1.20
PLA					
3251	0.58	1.79	0.33	0.748	1.00

Regression Equation

PLA

3001 Avg. TS (Mpa) = 44.83 - 0.00649 PEG - 0.735 WT (%)

3251 Avg. TS (Mpa) = 45.42 - 0.00649 PEG - 0.735 WT (%)

Fits and Diagnostics for Unusual Observations

Obs	Avg. TS (Mpa)	Fit	Resid	Std Resid	
7	20.00	27.33	-7.33	-2.03	R

R Large residual

Regression Analysis: Avg. YM (Gpa) versus PEG, WT (%), PLA

Method

Categorical predictor coding (1, 0)

Analysis of Variance

Source	DF	Adj SS	Adj MS	F-Value	P-Value
Regression	3	3.49570	1.16523	10.10	0.001
PEG	1	0.45492	0.45492	3.94	0.064
WT (%)	1	1.69038	1.69038	14.65	0.001
PLA	1	0.07172	0.07172	0.62	0.442
Error	16	1.84621	0.11539		
Total	19	5.34191			

Model Summary

S	R-sq	R-sq(adj)	R-sq(pred)
0.339688	65.44%	58.96%	46.17%

Coefficients

Term	Coef	SE Coef	T-Value	P-Value	VIF
Constant	2.889	0.204	14.14	0.000	
PEG	-0.000353	0.000178	-1.99	0.064	1.20
WT (%)	-0.0650	0.0170	-3.83	0.001	1.20
PLA					
3251	0.120	0.152	0.79	0.442	1.00

Regression Equation

PLA

3001 Avg. YM (Gpa) = 2.889 - 0.000353 PEG - 0.0650 WT (%)

3251 Avg. YM (Gpa) = 3.009 - 0.000353 PEG - 0.0650 WT (%)

Fits and Diagnostics for Unusual Observations

Obs	Avg. YM (Gpa)	Fit	Resid	Std Resid	
7	0.727	1.561	-0.834	-2.72	R

R Large residual

BIBLIOGRAPHY

- [1] “Overview of materials for Polylactic Acid (PLA) Biopolymer.” [Online]. Available: <http://matweb.com/search/DataSheet.aspx?MatGUID=ab96a4c0655c4018a8785ac4031b9278>. [Accessed: 19-Apr-2018].
- [2] V. M. Correlo, L. F. Boesel, M. Bhattacharya, J. F. Mano, N. M. Neves, and R. L. Reis, “Hydroxyapatite Reinforced Chitosan and Polyester Blends for Biomedical Applications,” *Macromol. Mater. Eng.*, vol. 290, no. 12, pp. 1157–1165, Dec. 2005.
- [3] “Overview of materials for PVC, Sheet Grade.” [Online]. Available: <http://www.matweb.com/search/DataSheet.aspx?MatGUID=7612abff891246f8aa0fb92a0e6ed522>. [Accessed: 23-Apr-2018].
- [4] M. Tobío, R. Gref, A. Sánchez, R. Langer, and M. J. Alonso, “Stealth PLA-PEG Nanoparticles as Protein Carriers for Nasal Administration,” *Pharm. Res.*, vol. 15, no. 2, pp. 270–275, Feb. 1998.
- [5] K. Kim *et al.*, “Incorporation and controlled release of a hydrophilic antibiotic using poly(lactide-co-glycolide)-based electrospun nanofibrous scaffolds,” *J. Controlled Release*, vol. 98, no. 1, pp. 47–56, Jul. 2004.
- [6] T. Serra, J. A. Planell, and M. Navarro, “High-resolution PLA-based composite scaffolds via 3-D printing technology,” *Acta Biomater.*, vol. 9, no. 3, pp. 5521–5530, Mar. 2013.
- [7] R. Scaffaro, F. Lopresti, L. Botta, S. Rigogliuso, and G. Gherzi, “Preparation of three-layered porous PLA/PEG scaffold: relationship between morphology, mechanical behavior and cell permeability,” *J. Mech. Behav. Biomed. Mater.*, vol. 54, pp. 8–20, Feb. 2016.
- [8] Y. K. Luu, K. Kim, B. S. Hsiao, B. Chu, and M. Hadjiargyrou, “Development of a nanostructured DNA delivery scaffold via electrospinning of PLGA and PLA-PEG block copolymers,” *J. Controlled Release*, vol. 89, no. 2, pp. 341–353, Apr. 2003.
- [9] T. Kaito *et al.*, “Potentiation of the activity of bone morphogenetic protein-2 in bone regeneration by a PLA-PEG/hydroxyapatite composite,” *Biomaterials*, vol. 26, no. 1, pp. 73–79, Jan. 2005.
- [10] S. S. Venkatraman, P. Jie, F. Min, B. Y. C. Freddy, and G. Leong-Huat, “Micelle-like nanoparticles of PLA-PEG-PLA triblock copolymer as chemotherapeutic carrier,” *Int. J. Pharm.*, vol. 298, no. 1, pp. 219–232, Jul. 2005.
- [11] J. Liu, “Reactive Extrusion of biodegradable Poly (lactic acid) and Polyester blends: Effects of PLA/EB062 ratio, Miscibility and Thermal Behavior,” University of Toledo, 2011.
- [12] M. R. Nanda, M. Misra, and A. K. Mohanty, “The Effects of Process Engineering on the Performance of PLA and PHBV Blends,” *Macromol. Mater. Eng.*, vol. 296, no. 8, pp. 719–728, Aug. 2011.
- [13] H. Sun, L. Mei, C. Song, X. Cui, and P. Wang, “The in vivo degradation, absorption and excretion of PCL-based implant,” *Biomaterials*, vol. 27, no. 9, pp. 1735–1740, Mar. 2006.

- [14] C. Gaball, S. Lovald, B. Baack, and G. Olson, “Minimally Invasive Bioabsorbable Bone Plates for Rigid Internal Fixation of Mandible Fractures,” *Arch. Facial Plast. Surg.*, vol. 13, no. 1, pp. 31–35, Jan. 2011.
- [15] “Fixation with Bioabsorbable Screws for the Treatment of Frac... : JBJS.” [Online]. Available: https://journals.lww.com/jbjsjournal/Abstract/1994/03000/Fixation_with_Bioabsorbable_Screws_for_the.1.aspx. [Accessed: 22-Apr-2018].
- [16] A. Colombo and E. Karvouni, “Biodegradable Stents: ‘Fulfilling the Mission and Stepping Away,’” *Circulation*, vol. 102, no. 4, pp. 371–373, Jul. 2000.
- [17] “Problem of Stress Shielding and Improvement to the Hip Implant Designs: A Review.” [Online]. Available: <https://scialert.net/abstract/?doi=jms.2007.460.467>. [Accessed: 22-Apr-2018].
- [18] O. Akkus, F. Adar, and M. B. Schaffler, “Age-related changes in physicochemical properties of mineral crystals are related to impaired mechanical function of cortical bone,” *Bone*, vol. 34, no. 3, pp. 443–453, Mar. 2004.
- [19] Y. C. Fung, *Biomechanics: Mechanical Properties of Living Tissues*. Springer Science & Business Media, 2013.
- [20] C. Öhman *et al.*, “Compressive behaviour of child and adult cortical bone,” *Bone*, vol. 49, no. 4, pp. 769–776, Oct. 2011.
- [21] “Titanium Ti-6Al-4V (Grade 5), Annealed.” [Online]. Available: <http://www.matweb.com/search/DataSheet.aspx?MatGUID=a0655d261898456b958e5f825ae85390>. [Accessed: 22-Apr-2018].

CURRICULUM VITAE

NAME: Jeremiah Bauer

ADDRESS: P.O. Box 14
Fort Knox KY,
40121

DOB: Heidelberg, Germany – November 12, 1993

**EDUCATION
& TRAINING** B.S., Mechanical Engineering
University of Louisville
2014-2016

Six Sigma Lean Green Belt (2347-7876)
IEEE
2016-2019